Reversible Thermodynamic Cycle Analysis for Capacitive Deionization with Modified Donnan Model

Li Wang[1], P.M. Biesheuvel[2], and Shihong Lin[1,3 *]

[1]Department of Civil and Environmental Engineering, Vanderbilt University, Nashville, TN 37235-1831, USA

[2]Wetsus, European Centre of Excellence for Sustainable Water Technology, Oostergoweg 9, 8911 MA Leeuwarden, The Netherlands

[3]Department of Chemical and Biomolecular Engineering, Vanderbilt University, Nashville, TN 37235-1604, USA

Abstract

It is a widely accepted principle that a thermodynamically reversible desalination process should consume the Gibbs free energy of separation. This principle has been shown in reverse osmosis and has important practical implications in reducing its energy consumption. Capacitive deionization (CDI) with carbon electrode, a desalination process based on electrical double layer (EDL) formation, should theoretically follow such a principle when it operates in a thermodynamically reversible way. Inspired by a previous thermodynamic analysis on a three-stage reversible CDI process using the Gouy-Chapman-Stern model, we conducted a thermodynamic analysis on a four-stage reversible CDI cycle using the modified Donnan model to better reflect the cyclic nature of practical CDI operations and account for the significant EDL overlap in nanosized micropores of realistic CDI electrodes. Our analysis on CDI cycles with different separations and final discharge voltage shows that electrical work to complete a four-stage cycles is numerically exactly identical to the Gibbs free energy of separation, as long as the cycle is operated in a thermodynamic reversible manner.

1. Introduction

Carbon electrode based capacitive deionization (CDI) utilizes the formation of electrical double layers (EDL) to temporarily store the charged ions in the micropores of the carbon electrodes. The capacity of temporary ion retention for a given mass of electrode is dependent on the cell voltage and will thus be eventually exhausted as more ions are stored in the electrodes[1-3]. Upon the saturation of carbon electrodes at a given cell voltage, one needs to recover the ion removal capacity by either short-circuiting the electrodes, or reducing the cell voltage, or even applying a reverse cell voltage, in which cases part or all of the temporarily stored ions are released back to the bulk solution.

To achieve an overall desalination separation, the system has to remove ions from the feed solution in the charging (or adsorption) stage, and to discharge these temporarily stored ions to the brine solution in the discharge (or desorption) stage, which is usually accomplished in two approaches in practical CDI operations. The first approach involves periodically feeding the CDI system with two streams from the same source water, one serving as the feed stream to be desalinated and the other as the brine stream to receive the discharged salts. Typical CDI configurations, such as flow-by and flow-through CDI[4, 5], belong to this approach. The second approach employs moving electrodes that are forced to be in alternating contact with the feed and brine streams for adsorption and desorption, respectively. CDI systems with flow electrodes[6, 7] or rotating-rod electrodes[8] belong to this approach. While systems adopting the first approach are structurally simpler and thus more prevalent, the second approach offers the advantages of continuous operation and a greater potential to desalinate high salinity feed stream.

Regardless of the operational approach, a CDI process always achieves a separation that is defined by the water recovery and the salinities of the feed solution, dilute solution, and brine solution. Solution thermodynamics dictates that a minimum amount of energy has to be consumed to achieve a given separation or, in other words, to achieve the non-spontaneous reduction of the solution entropy[9]. The minimum energy of separation, or the Gibbs free energy of separation, is consumed if and only if the separation process is thermodynamically reversible, whereas all practical processes involving thermodynamic irreversibility consume more energy than such a thermodynamic minimum[10]. This has been shown in reverse osmosis (RO) in which thermodynamic reversibility can be attained by adjusting the applied pressure to be always equal to the brine osmotic pressure[11, 12]. Demonstrating the same phenomenon (i.e. a reversible process consumes the minimum energy of separation) is significantly more challenging for CDI, but has nonetheless been successfully carried out with the Gouy-Chapman-Stern (GCS) model in a previous study[13].

Conducting a reversible thermodynamic analysis on a CDI process requires the quantification of equilibrium ion retention by the electrodes under different cell voltages[13]. The EDL theory suggests the existence of a well-defined relationship between the surface charge density and the surface potential when the EDL is in thermodynamic equilibrium[14]. For a planar surface with a fully developed EDL, the GCS model can be applied to relate the surface

potential to the areal surface charge density. In the GCS model, the EDL is decomposed into a charge-free Stern layer with a step potential drop and a diffuse layer the potential distribution of which is governed by the Poisson-Boltzmann (PB) equation[14, 15]. However, in realistic carbon electrodes used in CDI, micropores with a pore size of 2 nm and below are primarily responsible for ion retention[15, 16]. While the PB equation still applies within the framework of mean-field theory, the direct application of the GCS model in this case is challenging as EDLs cannot fully develop due to the geometric constraint, i.e., the EDLs significantly overlap in these micropores the dimension of which is comparable or even smaller than the Debye length[17]. This challenge of quantifying equilibrium ion retention in micropores has been overcome in recent CDI transport models by employing a modified Donnan (mD) model[18].

The previous study on a reversible CDI process analyzed a three-stage process comprising a charging stage, a solution switch stage, and a discharge stage[13]. It was shown that the as cell voltage returns to zero, the areal surface charge density also returns zero. However, in an mD model with micropores, the micropore solute concentration is dependent on the bulk solute concentration and can thus assume different values at zero cell voltage. This implies that while the previously analyzed three-stage CDI process appeared to be a cycle based on the relationship between charge density and cell voltage, it was not actually cyclic if the micropore solute concentration is also considered. While a non-cyclic process can also be thermodynamic reversible, a cyclic analysis is preferred to better reflect the nature of practical CDI operations.

This study aims to analyze the energy consumption of a thermodynamically reversible cycle for a CDI process using carbon electrodes with micropores. Specifically, we quantify the energy consumption a four-stage CDI cycle using the modified Donnan (mD) model and compare that to the Gibbs free energy of the separation achieved by such a cyclic CDI process. We derive the equilibrium relationships between cell voltage, volumetric charge density in the micropores, solute concentration in the micropores, and bulk concentration, based on the mD model. These equilibrium relationships, along with solute mass balance, are applied to analyze the energy consumption of four-stage batch CDI cycles. Finally, we compare the energy consumptions of these reversible CDI cycles with the Gibbs free energy of the separations resulting from those cycles.

2. Specific Gibbs free energy of separation

Regardless of the mechanism involved, a CDI process always separates the saline water (i.e. the feed solution) to a dilute solution and a concentrated solution (i.e. the brine). In general, we can define a separation by specifying the feed concentration, c_0, the dilute solution concentration, c_D, the brine concentration, c_B, and the water recovery, γ, which is simply the volume of the dilute solution over that of the feed solution (i.e. $\gamma = v_D/v_0$).

Of these four parameters that define a generic separation, only three are independent based on solute mass balance specified by eqn (1):

$$c_0 = c_B(1-\gamma) + c_D\gamma \quad (1)$$

A generic separation defined by c_0, c_D, c_B, and γ always requires a minimum amount of energy to generate a unit volume of the dilute solution as determined by reversible thermodynamics. This thermodynamically minimum energy is often referred to as the *specific* Gibbs free energy of separation, Δg, which can be quantified by computing the entropy change of the system induced by the separation[19]:

$$\Delta g = nRT\left\{\frac{c_0}{\gamma}\ln\left[\frac{c_0-\gamma c_D}{c_0(1-\gamma)}\right] - c_D\ln\left[\frac{c_0-\gamma c_D}{c_D(1-\gamma)}\right]\right\} \quad (2)$$

Here, n is the van't Hoff factor, R is the ideal gas constant, and T is the absolute temperature. Throughout the following discussion, we will focus on ideal solutions of 1:1 strong electrolytes (i.e. fully dissociated), rendering n =2. However, eqn (2) applies to any ideal solutions of strong electrolytes with any van't Hoff factor. We note that Δg, unlike the total Gibbs free energy of separation, is independent of the scale of desalination, thanks to the normalization by the volume of the dilute solution.

2. Modified Donnan (mD) model for ion retention by porous carbon electrodes

The mD model provides a very good approximation to the solution of the PB equation for micropores with a characteristic dimension smaller than or comparable to the Debye length[20]. It assumes a uniform potential distribution throughout the diffuse layer within the micropores, i.e., there is a single electrical potential instead of a potential distribution within the micropores (but outside the Stern plane)[21]. Two potential drops are present in the mD model: the Stern potential, $\Delta\phi_S$, which is the potential drop across the Stern layer; and the Donnan potential, $\Delta\phi_D$, which is a step potential drop across the micropore-macropore interface. For convenience, the mD model also uses volumetric charge density within the micropores, σ_{mi}, instead of the areal surface charge density that is more relevant to fully developed EDLs at solid-water interfaces. Moreover, the Stern layer capacitance, C_S, is assumed to be dependent on σ_{mi} [8, 18]. The mD model has been adopted for modeling ion retention performance for CDI[17, 18, 21, 22]. When the cell voltage, V_{cell}, is equally distributed between the two half cells, the relationship between σ_{mi} and V_{cell} at a given bulk concentration, c_∞, can be derived following the mD model presented below.

At equilibrium, the concentration of ion species i in the micropores ($c_{i,mi}$) is related to the Donnan potential and the macropore ion concentration according to

$$c_{i,mi} = c_{i,mA}\exp(-z_i\cdot\Delta\phi_D) \quad (3)$$

where $c_{i,mA}$ is the macropore concentration of ion i, z_i is the ion charge number (+1 for cations and -1 for anions), and $\Delta\phi_D$ is the dimensionless Donnan potential which can be multiplied by

the thermal voltage, V_t (i.e. 25.6 mV at room temperature) to obtain the actual Donnan potential with the unit Volt. Due to charge neutrality in macropores, $c_{i,mA}$ for the cation and anion equal each other and is also identical to the salt concentration (c_{mA}) for 1:1 electrolyte discussed. No differentiation is made between macropore and bulk in this analysis as equilibrium is maintained throughout the reversible thermodynamic process, i.e., the ion transport rate is infinitely slow such that no concentration gradient develops due to rate limited ion transport. Therefore, $c_{i,mA}$ is the same as the bulk concentration, c_∞.

For a 1:1 salt, the micropore volumetric charge density (σ_{mi}) is expressed as

$$\sigma_{mi} = \sum_i c_{i,mi} F = -2c_\infty \sinh(\Delta\phi_D)F \tag{4}$$

where F is the Faraday constant. The relationship between σ_{mi} and the dimensionless Stern layer potential, $\Delta\phi_S$, is given by

$$\sigma_{mi} = -C_{St,vol}\Delta\phi_S V_t \tag{5}$$

where $C_{St,vol}$ is the volumetric Stern layer capacitance. An empirical expression is often used to account for the increased Stern layer capacitance with increasing charge density due to electrostatic compression[23, 24].

$$C_{St,vol} = C_{St,vol,0} + \alpha(\sigma_{mi}/F)^2 \tag{6}$$

In equilibrium, the sum of $\Delta\phi_S$ and $\Delta\phi_D$ equals half of the potential across the cell ϕ_{cell} for symmetric cells

$$2(\Delta\phi_S + \Delta\phi_D) = V_{cell}/V_T \tag{7}$$

Here, potential drops due to resistances in the circuit, electrode, bulk solution and at the interfaces can be ignored because of the zero electrical current in a thermodynamically reversible process. Solving equations (3) to (7) yields the relationship between σ_{mi} and V_{cell} for a given c_{mA} (which is also c_∞ in equilibrium) when the system reaches thermodynamic equilibrium. Representative "σ_{mi} vs. V_{cell}" curves for c_∞ of 1, 10, and 100 mM are given in Fig. 1. The volumetric charge density, σ_{mi}, grows with increasing V_{cell}. At the same V_{cell}, σ_{mi} is higher with a higher bulk concentration, c_∞.

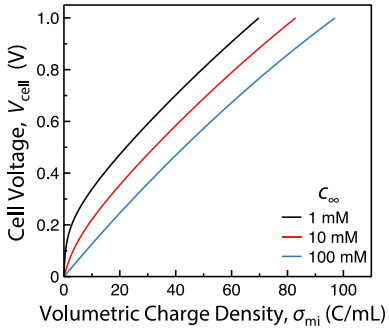

Figure.1 The quantitative relationship between cell voltage, V_{cell}, and the volumetric charge density in the micropores, σ_{mi}, when an electrode is in equilibrium with a bulk solution with different bulk salinity, c_∞. These curves are generated using the mD model given by eqns (3) to (7).

3. A four-stage reversible cycle for batch-mode capacitive deionization

The reversible thermodynamic cycle is composed of four stages: a charging stage, a discharge stage, and two stages responsible for switching the bulk solutions at the end of the charging and discharge stages. To facilitate discussion, we define four distinct states that are connected by, and demarcate, the four stages (Fig. 2). In addition, ideal carbon electrodes without intrinsic surface charges are assumed in this analysis[22], in other words, $\sigma_{mi} = 0$ if and only if $V_{cell} = 0$. Analysis of reversible thermodynamic cycle involving electrodes with intrinsic surface charge[22] or electrodes involving Faradaic reaction or ion intercalation[25, 26], which might be possible, is not considered in the current study. Here, we will describe, with the help of Fig. 2, the thermodynamic cycle in a batch operation using the four stages and the four states. We note that all processes described in the following text occur in an infinitely slow manner to maintain thermodynamic equilibrium throughout the process.

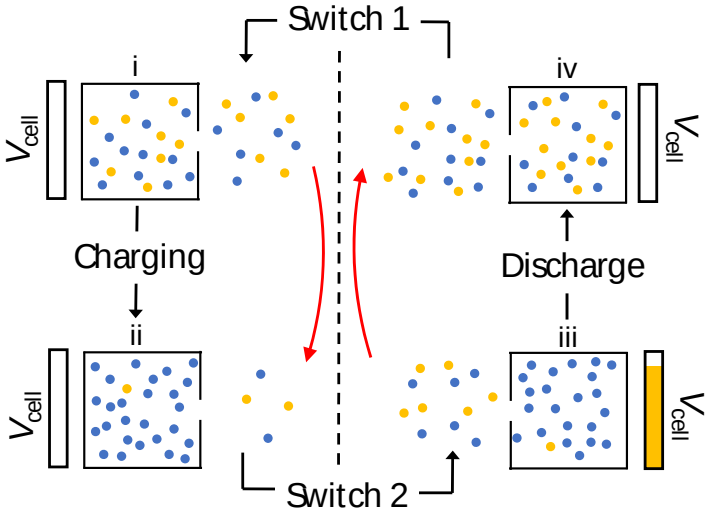

Figure 2. Graphical illustration of a batch-mode and thermodynamically reversible CDI process. The square box with a small opening represents the micropore the potential of which differs from the bulk solution (i.e. outside the micropores) by $\Delta\phi_D$. The areas of the micropore and bulk solution on the figure do not scale with their actual volumes in real systems. The progression from state (i) to (ii) represents the adsorption (charging) stage, whereas the progression from state (iii) to (iv) represents the desorption (discharge) stage. In the "switch 1" stage, the brine in the bulk solution is replaced by the feed solution, while the micropore concentration remains constant. In the "switch 2" stage, the dilute bulk solution is replaced by the feed solution that will receive the ions to be released from micropores, whereas the micropore concentration also remains constant. In both switching stages, the micropore salt concentrations, c_{mi}, are maintained to be constant by adjusting cell voltage, V_{cell}.

State (i) represents the point when bulk solution switching is completed and the system is ready for a new cycle of ion adsorption. In state (i), the bulk concentration, c_∞, is the feed concentration, c_0. However, the micropore concentration, $c_{mi,(i)}$, is maintained at the same micropore concentration as that before solution-switch ("Switch 1" in Fig. 2), i.e., based on our chosen assumption of fixed micropore concentration during solution-switch, $c_{mi,(i)}$ is equal to the c_{mi} in state (iv), $c_{mi,(iv)}$. The condition of constant c_{mi} can be achieved by varying V_{cell} to yield an $\Delta\phi_D$ that always equals $cosh^{-1}(c_{mi}/c_\infty)$ during the switch to maintain equilibrium.

The charging stage involves increasing V_{cell} to a predetermined maximum V_{cell} that defines state (ii). In state (ii), c_{mi} and σ_{mi} both reach maxima, whereas c_∞ attains minimum which is the concentration of the dilute solution, c_D. Once the charging stage is completed, the bulk solution at concentration c_D is switched to a new batch of bulk solution at concentration c_0. During this solution-switch ("Switch 2" in Fig. 2), the dilute solution is extracted from the system whereas the micropore concentration is maintained constant by reducing V_{cell} to maintain equilibrium. At the end of this solution-switch stage, the system is in state (iii).

The discharge stage is carried out by reducing V_{cell} to release the ions from the micropores to the bulk solution. In most cases, the cell voltage is reduced to zero at the end of the discharge stage, bringing the system to state (iv). The zero V_{cell} in state (iv) results in zero $\Delta\phi_D$ and zero micropore charge density, i.e. $\sigma_{mi,(iv)} = 0$. Consequently, the system in state (iv) has the same concentration for both micropore and the bulk solution, both being the brine concentration, c_B. We note that although here we introduce a reversible cycle with the V_{cell} in state (iv) being zero, the final discharge voltage can also be positive, in which case less retained ions are discharged.

The last stage of the cycle switches the bulk solution from the brine resulting in state (iv) to the feed solution with a concentration c_0, which is necessary for the next cycle CDI operation to begin. Here, V_{cell} is again controlled during this stage to maintain a constant micropore concentration (i.e. $c_{mi,(iv)} = c_{mi,(i)}$). This last solution-switch stage completes a CDI cycle. The system at the end of this switching stage is in state (i), which is also the beginning state of the next cycle. The net effect of a complete cycle elaborated above is the reduction of the salinity of a batch of feed solution from c_0 to c_D, and increasing the salinity of another batch of feed solution from c_0 to c_B (red arrows in Fig. 2), which is a separation completely defined by c_0, γ, c_B, and c_D. Certainly, energy has to be supplied to the system in order to run through this complete cycle.

To numerically construct the V_{cell}—σ_{mi} curve for a thermodynamic reversible CDI cycle describe above, we apply the mass balance equation about the solute as given by eqn (8):

$$(c_{mi}^0 - c_{mi})v_{mi} = (c_\infty - c_\infty^0)v_{bulk} \tag{8}$$

where c_{mi}^0 and c_∞^0 are the initial micropore and bulk concentrations respectively; c_{mi} and c_∞ are the micropore and bulk concentrations at any given time during the charging and discharge stages, which change as the charging/discharge occurs; v_{mi} is the total electrode micropore volume, and v_{bulk} is the bulk solution volume. It is worth noting that both initial concentrations refer to the state before either charging or discharge stage, which are also the concentrations at the end of either solution-switching stages. In the switching stages, c_{mi} remains constant while c_∞ decreases or increases to c_0 in 'switch 1' or 'switch 2', respectively. The cell voltage is continuously adjusted to maintain an equilibrium between micropore and macropore.

Eqns (3) to (8), which are essentially based on equilibrium condition and solute mass balance, are solved numerically to construct a full cycle consisting of charging, discharge, and two solution-switch stages. A reversible cycle can be presented using two separate figures, one

showing the relationship between V_{cell} and σ_{mi} and the other showing the relationship between c_{mi} and c_∞. In this study, the final charging voltage is chosen to be 1V, whereas zero and non-zero voltage discharge are both investigated.

4. Reversible CDI cycles consume Gibbs free energy of separation

Fig. 3 shows the "V_{cell} vs. σ_{mi}" and "c_{mi} vs. c_∞" curves for two representative separations. The first separation (Fig. 3A and 3B) reduces the salinity of 90% of the feed solution from 20 mM to 0.5 mM, converting 10% of the feed water into a brine with a salinity of 195.5 mM. The specific Gibbs free energy of separation, Δg, calculated using eqn (2), is 0.066 kWh m^{-3}. The second separation (Fig. 3C and 3D) recovers 50% of feed solution to become a dilute solution of 1 mM, turning the other 50% of the feed water to be a brine solution of 39 mM, which requires a Δg of 0.032 kWh m^{-3}.

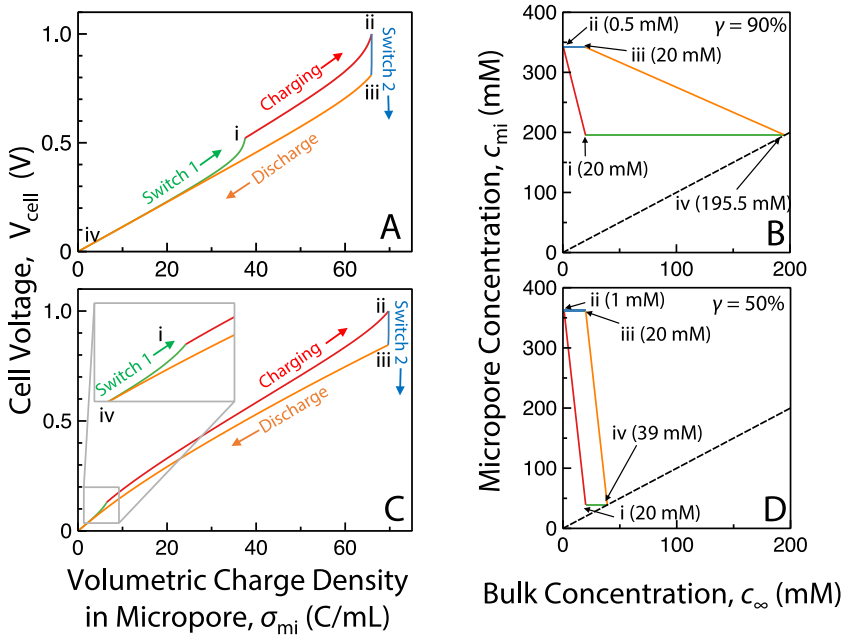

Figure 3. (A) and **(C)** the relationship between volumetric charge density in the micropores, σ_{mi}, and the cell voltage, V_{cell}, in thermodynamically reversible CDI cycles. **(B)** and **(D)** the relationship between micropore concentration, c_{mi}, and the bulk concentration, c_∞, in the corresponding reversible CDI cycles. The dashed lines in **(B)** and **(D)** represent cases where c_{mi} is equal to c_∞. The separation described by (A) and (B) is defined as c_0=20 mM, c_D=0.5 mM, c_B=195.5 mM and γ=90%. The separation described by **(C)** and **(D)** is defined as c_0=20 mM, c_D=1 mM, c_B=39 mM and γ=50%. The four states (i, ii, iii, and iv) and the four stages (featured by different colors) are shown in the figures. Each point on the cycles is derived using the mD model to establish the relation between σ_{mi} and V_{cell} at a given c_∞. However, unlike Fig. S1, each point on the cycles corresponds to a different bulk salinity, c_∞, to account for the change of the bulk solution during the charging/discharging and switch stages. SEC of a reversible CDI cycle is proportional to the area outlined by the respective cycles **(A)** and **(C)**.

The total electrical work required to run such thermodynamic reversible CDI cycles, W_R, can be determined by subtracting the electrical work done by the system during the discharge stage (W_d) and the second switching stage (W_{s2}) from the electrical work done to system during the first switching stage (W_{s1}) and the charging stage (W_c), i.e., $W_R = W_{s1} + W_c - W_{s2} - W_d$.

This can be quantified by multiplying the total micropore volumes, v_{mi}, with the area of the "cycles" in Fig. 2A and 2C, which represent the electrical work done to the system per micropore volume. Specific energy consumption (*SEC*) of such a reversible CDI cycle, SEC_R, is defined as the energy consumed per volume of dilute solution:

$$SEC_R = \frac{W_R}{v_D} = \frac{v_{mi}}{v_D} \oint V_{cell}(\sigma_{mi}) d\sigma_{mi} \tag{9}$$

We note that no system-specific parameter is needed when quantifying SEC_R using eqn (9) except the two parameters used in the empirical expression for the volumetric Stern layer capacitance, $C_{St,vol}$. The values of these parameters ($C_{St,vol,0}$ and α in eqn (6)), which are determined mostly by the physics of the Stern layer rather than the properties of the materials and are thus relatively universal, are chosen according to what have been reported in literature[18, 27].

Numerical integrations were carried out to find SEC_R, based on eqn (9), for both separations presented in Fig.3. SEC_R for the first separation (Fig. 3A and 3B) and the second separation (Fig. 3C and 3D) are found to be 0.066 and 0.032 kWh m^{-3}, respectively. These SEC_R, calculated using eqn (9), are almost exactly the same as Δg for the respective separations calculated using eqn (2), with less than 0.3% numerical deviation. This exceptional numerical consistence between SEC_R and Δg demonstrates that a thermodynamically reversible CDI processes consume Gibbs free energy of separation.

The thermodynamic cycle analysis can also be conducted on a CDI process in which the final voltage of the discharge stage is positive. Such an incomplete discharge is relevant as it has been shown that increased discharge voltage can enhance charge efficiency and reduce energy consumption in practical operations[28]. Fig. 4 shows a CDI cycle with a final discharge voltage of 0.7 V (solid cycle) as compared to a reference cycle with a final discharge voltage of 0 (dotted cycle).

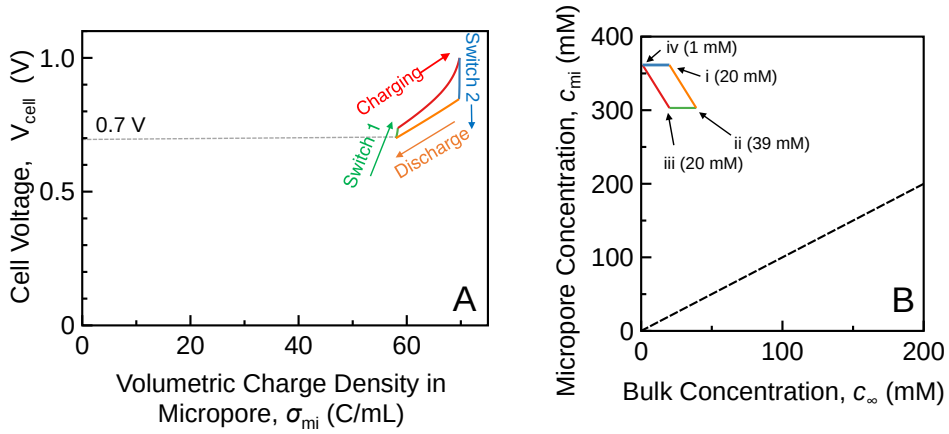

Figure 4. The relationships betwee (A) σ_{mi} and V_{cell}, and **(B)** c_{mi} and c_∞, in a thermodynamically reversible CDI cycle. The separation is defined as c_0=20 mM, c_D=1 mM, c_B=39 mM and γ=50%. The final voltage of the discharge stage is 0.7 V as shown in Figure 4A. The reference cycle presented using dotted lines/curves is the same as that in Fig. 3, which achieves the same separation but with a final discharge voltage of 0V.

Because the difference between the initial and final σ_{mi} for the charging stage in this case is significantly lower than that in a CDI cycle with a final discharge voltage of 0V, the CDI cycle in Fig. 4 requires a significantly larger micropore volume (equivalent to more electrode mass) per volume of dilute solution to achieve the same separation attained using a CDI cycle fully discharged to zero voltage. Therefore, even though the integrals $\oint V_{cell}(\sigma_{mi})d\sigma_{mi}$ is significantly smaller for a CDI cycle with a final discharge voltage of 0.7 V, as shown in Fig. 4A, than that for CDI cycle with a final discharge voltage of 0, the SEC_R in these two CDI processes turn out to be exactly the same after accounting for the different v_{mi}.

The exceptional numerical consistence between SEC_R and Δg is not limited to the three specific scenarios discussed above. We have tested several other CDI cycles with different resulting separations and the numerical consistence between SEC_R and Δg is observed in all cases (Fig. 5). So far, we have yet to observe any negative example in which such a numerical consistence does not apply.

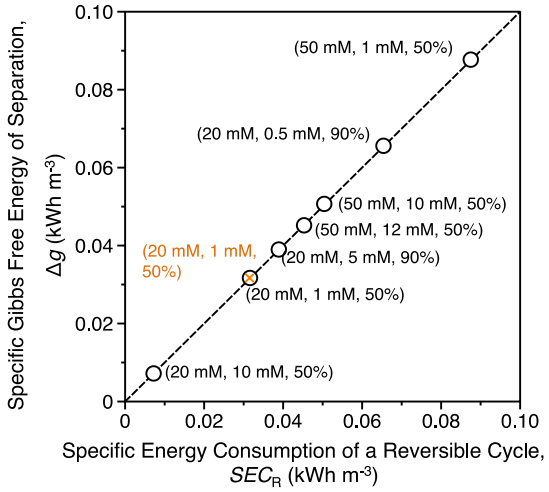

Figure5. Specific Gibbs free energy of separation, Δg, vs. specific energy consumption of a reversible CDI cycle, SEC_R for different separations. Each separation is defined by c_0, c_D, and γ that are given in the parentheses. All but the organe "x" are results from CDI cycles with a zero final discharge voltage. The organe "x" results from a CDI cycle with a final discharge voltage of 0.7 V. In all cases, the final voltage of the charging stage is 1 V. The dashed line represents the scenarios in which Δg is exactly equal to SEC_R. The linear regression of the data yileds a correlation (not shown in figure) of Δg=1.0024 SEC_R+0.00002, with an R^2 of 0.99998.

Admittedly, we cannot derive an analytical expression of SEC_R for a thermodynamically reversible CDI cycle and compare that to the analytical expression of Δg, as what has been done for RO[12, 29, 30] and pressure retarded osmosis (PRO) [31]. Nor can we exhaustively verify the numerical consistence between SEC_R and Δg for all possible separations. However, results from the mD model seem to provide confident support toward the widely-accepted principle that a separation process, if operated thermodynamically reversibly, consumes the Gibbs free energy of separation.

5. Concluding Remarks

Analysis of thermodynamically reversible, four-stage batch CDI cycles using the mD model suggests that the electrical work consumed in such those reversible cycles are identical to the Gibbs free energy of the separations resulting from those cycles. Such an equality between SEC_R and Δg holds for all investigated scenarios with different feed salinity, dilute solution salinity, water recovery, and final discharge voltage. On the one hand, this equality is anticipated according to the widely recognized thermodynamic principle that a reversible separation process consumes the Gibbs free energy of separation. For example, such an equality has been demonstrated analytically in RO and PRO. It would be surprising if our analysis suggests otherwise.

On the other hand, it is rather impressive that numerical analyses based on the mD model in this study, and the GCS model in a previous study, both yield results that abide by this theoretically predicted equality to an exceptional precision. After all, both models only provide mean-field approximations of the realistic ion distribution in an EDL, and are based on empirical estimation of the Stern capacitance. While it is mechanistically very clear about how we arrived in such an equality for separating ideal solutions by RO, the fact that we can demonstrate this expected equality using numerical models with empirical parameters is both surprising and theoretically reassuring. Finally, the analysis of a thermodynamically reversible RO process has provided important insights to reduction of energy consumption in RO practice via innovative operation such as multi-stage and closed-circuit RO. We expect the elucidation of the thermodynamically reversible CDI cycle may also serve the theoretical foundation for us to better understand sources of inefficiency in practical CDI processes, and to develop novel operations or justify existing operations with higher thermodynamic reversibility and thus high energy efficiency.

Acknowledgement

The author S.Lin acknowledge the support from Oak Ridge Associated Universities (ORAU) through the Ralph E. Powe Jr Faculty Enhancement Award.

Reference

[1] Y. Oren, Capacitive delonization (CDI) for desalination and water treatment - past, present and future (a review), Desalination 228 (2008) 10-29.
[2] M.A. Anderson, A.L. Cudero, J. Palma, Capacitive deionization as an electrochemical means of saving energy and delivering clean water. Comparison to present desalination practices: Will it compete?, Electrochim Acta 55 (2010) 3845-3856.
[3] S. Porada, R. Zhao, A. van der Wal, V. Presser, P.M. Biesheuvel, Review on the science and technology of water desalination by capacitive deionization, Prog Mater Sci 58 (2013) 1388-1442.
[4] J.C. Farmer, D.V. Fix, G.V. Mack, R.W. Pekala, J.F. Poco, Capacitive deionization of NaCl and NaNO3 solutions with carbon aerogel electrodes, J Electrochem Soc 143 (1996) 159-169.

[5] M.E. Suss, T.F. Baumann, W.L. Bourcier, C.M. Spadaccini, K.A. Rose, J.G. Santiago, M. Stadermann, Capacitive desalination with flow-through electrodes, Energ Environ Sci 5 (2012) 9511-9519.
[6] S. Porada, D. Weingarth, H.V.M. Hamelers, M. Bryjak, V. Presser, P.M. Biesheuvel, Carbon flow electrodes for continuous operation of capacitive deionization and capacitive mixing energy generation, J Mater Chem A 2 (2014) 9313-9321.
[7] S.I. Jeon, H.R. Park, J.G. Yeo, S. Yang, C.H. Cho, M.H. Han, D.K. Kim, Desalination via a new membrane capacitive deionization process utilizing flow-electrodes, Energ Environ Sci 6 (2013) 1471-1475.
[8] S. Porada, B.B. Sales, H.V.M. Hamelers, P.M. Biesheuvel, Water Desalination with Wires, J Phys Chem Lett 3 (2012) 1613-1618.
[9] A. Bejan, Advanced Engineering Thermodynamics, 2nd ed., Wiley1997.
[10] K.S. Spiegler, Y.M. El-Sayed, The energetics of desalination processes, Desalination 134 (2001) 109-128.
[11] M. Elimelech, W.A. Phillip, The Future of Seawater Desalination: Energy, Technology, and the Environment, Science 333 (2011) 712-717.
[12] A.Z. Zhu, P.D. Christofides, Y. Cohen, Effect of Thermodynamic Restriction on Energy Cost Optimization of RO Membrane Water Desalination, Ind Eng Chem Res 48 (2009) 6010-6021.
[13] P.M. Biesheuvel, Thermodynamic cycle analysis for capacitive deionization, Journal of colloid and interface science 332 (2009) 258-264.
[14] E.J. Verwey, J.T.G. Overbeek, Theory of the stability of Lyophobic Colloids, Dover Publications1999.
[15] R.J. Hunter, Foundations of Colloid Science, 2nd Edition ed., Oxford University Press2001.
[16] C. Lin, J.A. Ritter, B.N. Popov, Correlation of double-layer capacitance with the pore structure of sol-gel derived carbon xerogels, J Electrochem Soc 146 (1999) 3639-3643.
[17] P.M. Biesheuvel, R. Zhao, S. Porada, A. van der Wal, Theory of membrane capacitive deionization including the effect of the electrode pore space, Journal of colloid and interface science 360 (2011) 239-248.
[18] S. Porada, L. Weinstein, R. Dash, A. van der Wal, M. Bryjak, Y. Gogotsi, P.M. Biesheuvel, Water Desalination Using Capacitive Deionization with Microporous Carbon Electrodes, Acs Appl Mater Inter 4 (2012) 1194-1199.
[19] S.I. Sandler, Chemical, Biochemical and Engineering Thermodynamics, 4 th ed., Wiley2006.
[20] S. Porada, L. Borchardt, M. Oschatz, M. Bryjak, J.S. Atchison, K.J. Keesman, S. Kaskel, P.M. Biesheuvel, V. Presser, Direct prediction of the desalination performance of porous carbon electrodes for capacitive deionization, Energ Environ Sci 6 (2013) 3700-3712.
[21] P.M. Biesheuvel, S. Porada, M. Levi, M.Z. Bazant, Attractive forces in microporous carbon electrodes for capacitive deionization, J Solid State Electr 18 (2014) 1365-1376.
[22] P.M. Biesheuvel, H.V.M. Hamelers, M.E. Suss, Theory of Water Desalination by Porous Electrodes with Immobile Chemical Charge, Colloid Interfac Sci 9 (2015) 1-5.
[23] D.J. Bonthuis, S. Gekle, R.R. Netz, Dielectric Profile of Interfacial Water and its Effect on Double-Layer Capacitance, Phys Rev Lett 107 (2011).
[24] M.Z. Bazant, K.T. Chu, B.J. Bayly, Current-voltage relations for electrochemical thin films, Siam J Appl Math 65 (2005) 1463-1484.
[25] K.C. Smith, Theoretical evaluation of electrochemical cell architectures using cation intercalation electrodes for desalination, Electrochim Acta 230 (2017) 333-341.
[26] M. Pasta, C.D. Wessells, Y. Cui, F. La Mantia, A Desalination Battery, Nano Lett 12 (2012) 839-843.
[27] H. J, Q. R, F. G, S. BG, M. V, Modern Theories of Carbon-Based Electrochemical Capacitors, Wiley, New York, 2013.
[28] T. Kim, J.E. Dykstra, S. Porada, A. van der Wal, J. Yoon, P.M. Biesheuvel, Enhanced charge efficiency and reduced energy use in capacitive deionization by increasing the discharge voltage, Journal of colloid and interface science 446 (2015) 317-326.
[29] M.H. Li, Reducing specific energy consumption in Reverse Osmosis (RO) water desalination: An analysis from first principles, Desalination 276 (2011) 128-135.
[30] S.H. Lin, M. Elimelech, Kinetics and energetics trade-off in reverse osmosis desalination with different configurations, Desalination 401 (2017) 42-52.
[31] N.Y. Yip, M. Elimelech, Thermodynamic and Energy Efficiency Analysis of Power Generation from Natural Salinity Gradients by Pressure Retarded Osmosis, Environ Sci Technol 46 (2012) 5230-5239.

399